PCCP

ROYAL SOCIETY OF CHEMISTRY

PAPER

View Article Online
View Journal | View Issue

Cite this: *Phys. Chem. Chem. Phys.*, 2021, **23**, 22096

Vacuum ultraviolet photochemistry of the conformers of the ethyl peroxy radical†

Zuoying Wen,‡[a] Xiaoxiao Lin,‡[a] Xiaofeng Tang,*[a] Bo Long,[b] Chengcheng Wang,[a] Cuihong Zhang,[a] Christa Fittschen,[c] Jiuzhong Yang,[d] Xuejun Gu[a] and Weijun Zhang*[a]

Received 13th June 2021,
Accepted 7th September 2021

DOI: 10.1039/d1cp02655k

rsc.li/pccp

We study the conformers of the ethyl peroxy radical ($C_2H_5O_2$), the simplest peroxy radical having more than one conformer, by combining synchrotron radiation vacuum ultraviolet (VUV) photoionization mass spectrometry with theoretical calculations. The ethyl peroxy radical is formed in a microwave discharge flow tube through the reaction of the ethyl radical (C_2H_5) with oxygen molecules, where C_2H_5 is generated *via* the hydrogen-abstraction reaction of ethane with fluorine atoms. Two kinds of $C_2H_5^+$, originating from photoionization of C_2H_5 and from dissociative photoionization of $C_2H_5O_2$, whose cation is not stable, have been identified and separated in photoionization mass spectra. The photoionization spectrum corresponding to $C_2H_5O_2$ is obtained and assigned with Franck–Condon calculations. The present findings show that the *gauche* conformer (*G*-$C_2H_5O_2$) of $C_2H_5O_2$ has favorable Franck–Condon factors in the ionization transitions, whereas the contribution of the *trans* conformer (*T*-$C_2H_5O_2$) to the photoionization spectrum is minor or negligible due to its large geometric changes in the photoionization process. Moreover, the reason for the instability of $C_2H_5O_2^+$ and its detailed dissociation mechanisms have been unraveled with the aid of the calculated potential energy curves.

1. Introduction

Peroxy radicals (RO_2) are very important reaction intermediates that play crucial roles in the low temperature oxidation of organic compounds in combustion and atmospheric chemistry.[1–3] In the atmosphere, peroxy radicals are formed *via* the reaction of alkyl radicals (R) with oxygen molecules. Then the formed peroxy radicals can undergo bimolecular reactions with various species, such as NOx (NO and NO_2), HO_2 and other peroxy radicals, self-reaction and unimolecular reaction. These key processes make an important contribution for the production of secondary pollutants such as ozone and secondary organic aerosols (SOA).[2,3] Thus the direct measurement of peroxy radicals is a fundamental issue in atmospheric chemistry.

The spectroscopy and structure of peroxy radicals are of considerable importance for understanding their reactivity, sources and sinks in the atmosphere. In the past decades, benefiting from the constant development of analytical methods such as absorption spectroscopy,[4,5] cavity ring-down spectroscopy (CRDS),[6–9] photoionization mass spectrometry (PIMS)[10,11] and photoelectron photoion coincidence spectroscopy (PEPICO),[12,13] a great deal of advance has been made to unravel their spectroscopy and structures. Among them, PIMS and PEPICO in particular combined with tunable synchrotron radiation as the photoionization light source have attracted attention and are considered as universal and sensitive methods to probe and analyze such elusive species.[14–16] For example, Meloni *et al.* studied the vacuum ultraviolet (VUV) photoionization of alkylperoxy radicals at the Advanced Light Source by using PIMS and found most of their cations unstable except for the methyl peroxy radical (CH_3O_2).[10] The ionization energy (IE) of CH_3O_2 and the appearance energy (AE) of the CH_3^+ fragment ion in dissociative photoionization of CH_3O_2 were measured using PEPICO by Voronova *et al.* at the Swiss Light Source and Tang *et al.* at SOLEIL, France.[12,13]

With the increase in mass, the structure of peroxy radicals becomes complex, having several isomers or conformers. For instance, the ethyl peroxy radical has two conformers, the *gauche* conformer (*G*-$C_2H_5O_2$) with its CCOO dihedral angle of $\pm 60^\circ$ and the *trans* conformer (*T*-$C_2H_5O_2$) with the CCOO

[a] *Laboratory of Atmospheric Physico-Chemistry, Anhui Institute of Optics and Fine Mechanics, HFIPS, Chinese Academy of Sciences, Hefei, 230031 Anhui, China. E-mail: tangxf@aiofm.ac.cn, wjzhang@aiofm.ac.cn*
[b] *School of Materials Science and Engineering, Guizhou Minzu University, Guiyang, 550025 Guizhou, China*
[c] *University Lille, CNRS, UMR 8522, PC2A – Physicochimie des Processus de Combustion et de l'Atmosphère, F-59000 Lille, France*
[d] *National Synchrotron Radiation Laboratory, University of Science and Technology of China, Hefei, 230029 Anhui, China*

† Electronic supplementary information (ESI) available. See DOI: 10.1039/d1cp02655k

‡ These authors contributed equally to this work.

dihedral angle of ±180°, and the propyl peroxy radical has two isomers, 1-$C_3H_7O_2$ and 2-$C_3H_7O_2$, each of which also has several conformers.[6] The knowledge on the isomers or conformers of peroxy radicals is very limited, and identifying them is still a challenge. Recently, using the method of PEPICO at SOLEIL, two isomers of $C_3H_7O_2$ were successfully identified and assigned in our publication.[17]

Here we focus on the ethyl peroxy radical, $C_2H_5O_2$, and its two conformers, *G*-$C_2H_5O_2$ and *T*-$C_2H_5O_2$. The ethyl peroxy radical is the simplest peroxy radical having more than one conformer, and has attracted attention.[18–21] Previous theoretical calculations showed that *G*-$C_2H_5O_2$ is the global minimum with an energy of ~80 cm^{-1} lower than *T*-$C_2H_5O_2$.[20,21] Upon photoionization, the nascent $C_2H_5O_2^+$ cation is not stable and dissociates to $C_2H_5^+$ and O_2 fragments.[10,11] To explain the instability of $C_2H_5O_2^+$, Meloni *et al.* suggested the cation has a hyper-conjugation structure.[10] The AE of the $C_2H_5^+$ and O_2 fragments was measured at 10.0 ± 0.1 eV in the photoionization spectrum by these authors.

In this work, VUV photoionization of $C_2H_5O_2$ has been investigated in detail by using synchrotron-based PIMS complemented by high-level theoretical calculations on the IEs, structures and spectra. After distinguishing two different sources of $C_2H_5^+$, originating from the photoionization of the ethyl radical (C_2H_5) and from the dissociative photoionization of $C_2H_5O_2$, the photoionization spectrum corresponding to $C_2H_5O_2$ is acquired and has been assigned with Franck–Condon calculations. The present findings will demonstrate that the *G*-$C_2H_5O_2$ conformer has favorable Franck–Condon factors in the ionization transition, whereas the contribution of *T*-$C_2H_5O_2$ to the photoionization spectrum is minor or negligible due to its large geometric changes in the photoionization process.

2. Methods

The experiments were carried out on the combustion and flame beamline at National Synchrotron Radiation Laboratory (NSRL) in Hefei, China.[22] A fast flow tube was employed as the reactor to generate free radicals and initiate their chemical reactions.[23] A home-made photoionization orthogonal acceleration reflectron time-of-flight (TOF) mass spectrometer was installed to probe and analyze reactants, reaction intermediates and products inside the fast flow tube.[24] The detailed configurations of the synchrotron beamline, the fast flow tube and the TOF mass spectrometer have already been introduced before and only a brief description is presented here.[22–24]

Briefly, on the beamline, synchrotron photons emitted from an undulator were dispersed by a monochromator equipped with two gratings, 200 and 400 l mm^{-1}, covering the photon energy range of 5–21 eV. A gas filter presently filled with Ar gas was adopted to suppress high-order harmonic radiations from the undulator, and the absolute photon energy was calibrated within an accuracy of ±10 meV using the resonant absorption lines of Ar in the gas filter.[25] The synchrotron photon flux was measured using a photodiode (SXUV-100, IRD Inc.) and used to normalize ion signals in the photon energy scans.

The fast flow tube mainly including a main tube and a coaxial movable injector was installed inside the source chamber of the TOF mass spectrometer.[23] Fluorine atoms were generated from 1% diluted F_2 gas in helium using a 2.45 GHz microwave discharge generator (GMS-200W, Sairem, France) and introduced into the fast flow tube to initiate chemical reactions. Other reactant gases such as ethane and oxygen, together with helium bath gas, were injected *via* the arms of the main tube or the injector. The total pressure inside the flow tube was monitored using a capacity gauge and fixed at 2 Torr by using a closed-loop feedback throttle valve.

After passing through one skimmer (1 mm diameter), the gas mixture in the fast flow tube was sampled and entered into the ionization chamber of the TOF mass spectrometer, crossing a synchrotron photon beam at a right angle and then being ionized. A cage-shaped photoionization source connected with an Einzel lens was developed to extract and focus ions, and then to enhance the detection sensitivity of the setup.[24] The TOF mass spectrometer with an orthogonal acceleration and reflectron structure was employed to analyze the mass of ions. The total ion flight length was ~1 m and the mass resolving power of the TOF mass spectrometer was measured to be $M/\Delta M$ ~ 2000 (FWHM, the full width at half maximum).[24]

To provide further insights into the experimental data, theoretical calculations have been performed to study the adiabatic ionization energies (AIEs), the potential energy curves and the Franck–Condon factors, using the Gaussian 16 package and MOLPRO 2015 software.[26,27] The geometric structures of the two conformers of $C_2H_5O_2$ and their cations were optimized by using the M06-2X/aug-cc-pVTZ theoretical methods. The AIEs of the two conformers were calculated using the explicitly correlated coupled cluster single-double and perturbative triple excitations approach, (R)CCSD(T)-F12/aug-cc-pVTZ.[27] The potential energy curves of the low-lying electronic states of neutral $C_2H_5O_2$ and its cation along the C–O coordinates have been calculated at the M06-2X/aug-cc-pVTZ level. In order to assign the photoionization spectrum of $C_2H_5O_2$, the Franck–Condon factors in the ionization transitions have been calculated at the M06-2X/aug-cc-pVTZ level too, using the time-independent adiabatic Hessian Franck–Condon model in the Gaussian program.[26]

3. Results and discussion

The experiments were performed in sequence and can be divided into two parts. At first, the experiment was carried out without adding oxygen gas into the fast flow tube, and the ethyl radical (C_2H_5) was produced *via* the hydrogen-abstraction reaction of ethane with fluorine atoms.

$$F + C_2H_6 \rightarrow C_2H_5 + HF \quad (1)$$

Secondly, with the addition of oxygen gas, the nascent ethyl radical reacted with oxygen to generate the products, $C_2H_5O_2$,

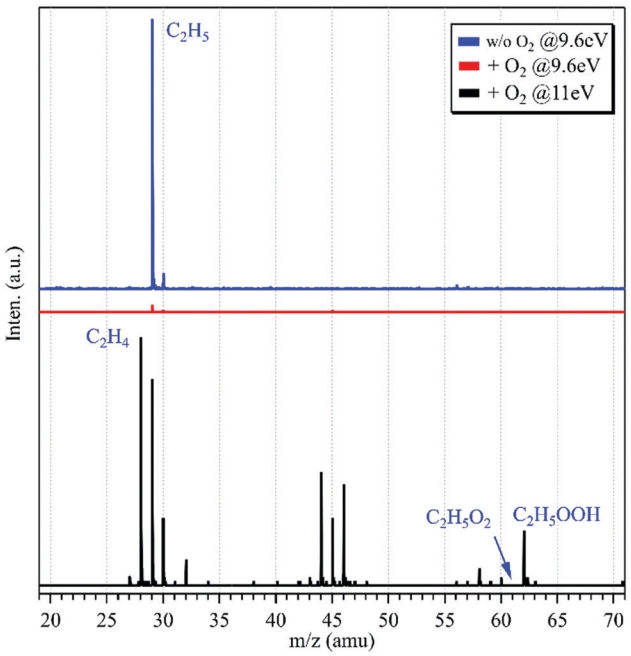

Fig. 1 Photoionization TOF mass spectra acquired without (in blue, $h\nu$ = 9.6 eV) and with (in red, $h\nu$ = 9.6 eV; in black, $h\nu$ = 11.0 eV) the addition of oxygen into the fast flow tube.

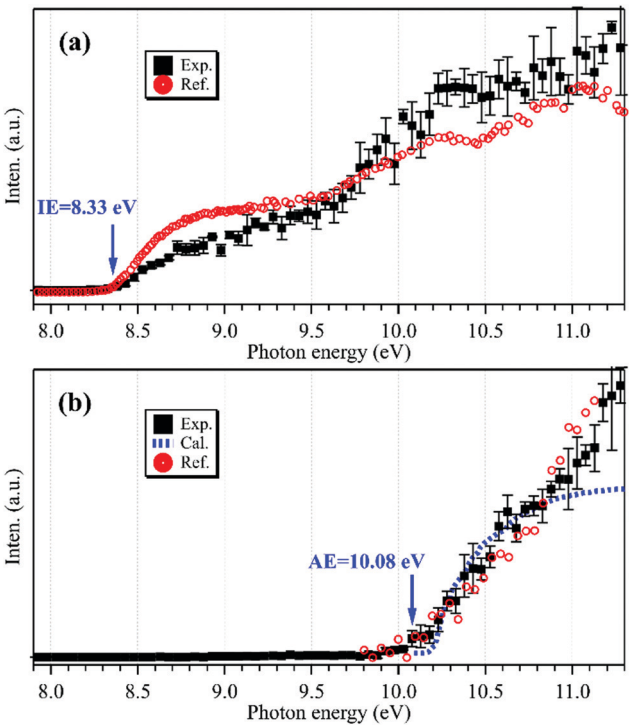

Fig. 2 Photoionization spectra of the m/z = 29 cations acquired without (a) and with (b) the addition of oxygen gas into the flow tube, together with the reference data of C_2H_5 (a, in red) reprinted from Ruscic *et al.*[30] (with the permission of AIP Publishing), the reference data of $C_2H_5O_2$ (b, in red) adapted from Meloni *et al.*[10] (Copyright 2021 American Chemical Society), and the calculated results of $C_2H_5O_2$ (b, in blue).

ethylene (C_2H_4) and the hydroperoxy radical (HO_2), *via* the following two reactions.[19,28]

$$C_2H_5 + O_2 \rightarrow C_2H_5O_2 \quad (2a)$$

$$\rightarrow C_2H_4 + HO_2 \quad (2b)$$

The photoionization mass spectrum in the absence of oxygen in the fast flow tube was acquired at the photon energy of $h\nu$ = 9.6 eV and is presented as a blue line in Fig. 1. An intense peak is observed at m/z = 29 and has been assigned as C_2H_5 produced from the above mentioned hydrogen-abstraction reaction (1). Another mass peak at m/z = 30 is observed in the mass spectrum too, and can be ascribed to the $^{13}C_2H_5$ isotopic ethyl radical with an intensity of about 4% of the m/z = 29 peak. The IE of ethane locates at 11.52 eV,[29] above the present photon energy of 9.6 eV, indicating that ethane does not contribute to the m/z = 30 peak.

The photoionization spectrum of C_2H_5 has been measured by scanning the synchrotron photon energy with a step size of 0.05 eV, and is presented as black squares in Fig. 2(a). The overall shape of the photoionization spectrum is similar to the literature results of Ruscic *et al.*,[30] and the difference might be due to the different internal energies of the produced ethyl radicals and the different photo-flux calibrations in the two experiments. Presently the cationic signal appears at $h\nu$ = 8.33 ± 0.05 eV in the photoionization spectrum, in accordance with the IE of C_2H_5.[29,31]

After adding oxygen gas into the flow tube, the intensity of the m/z = 29 mass peak declines, nearly approaching the baseline of the mass spectrum, as shown using a red line in Fig. 1. In addition, almost no other peaks can be observed in the mass spectrum. Previous results have shown that the reaction of C_2H_5 with oxygen is fast with a rate constant of 2×10^{-12} cm^3 molecule^{-1} s^{-1} at 298 K,[32] and can generate the products of $C_2H_5O_2$, C_2H_4 and HO_2. The $C_2H_5O_2^+$ cation is not stable and the AE of the $C_2H_5^+$ and O_2 fragments was measured at 10.0 ± 0.1 eV,[10] above the present photon energy of 9.6 eV. For the other products, C_2H_4 and HO_2, their IEs locate at 10.5138 and 11.359 eV,[29] respectively, and thus they are not observed in the mass spectrum.

The synchrotron photon energy was increased to $h\nu$ = 11.0 eV, and the photoionization mass spectrum was acquired and is presented as a black line in Fig. 1. Similar to the previous results,[10,11] still no signal could be observed at m/z = 61 ($C_2H_5O_2^+$) in the mass spectrum. But, presently the m/z = 29 mass peak appears again and this reappearance should have a different source as that of the above C_2H_5 obtained in the absence of O_2. In addition, the product of C_2H_4 (m/z = 28) from the reaction of C_2H_5 with oxygen has been observed in the mass spectrum. Some other peaks are observed in the mass spectrum too and can be ascribed to the secondary reactions occurring in the flow tube.[33] For example, the m/z = 30 mass peak is ascribed to the secondary reaction product of HCHO whose IE is measured at 10.83 ± 0.05 eV in the photoionization spectrum (Fig. S1, ESI†), and the m/z = 62 mass peak can be assigned as C_2H_5OOH, the product of the reaction of $C_2H_5O_2$ with HO_2.

To explain the reappearance of the m/z = 29 peak in the mass spectrum, its photoionization spectrum was acquired (with the

addition of oxygen) and is presented as black squares in Fig. 2(b), together with the literature data of Meloni *et al.*[10] Unlike the case in Fig. 2(a), presently the m/z = 29 cation does not appear until at $h\nu$ = 10.08 ± 0.05 eV in the photoionization spectrum, agreeing well with the literature, AE($C_2H_5^+$) = 10.0 ± 0.1 eV in dissociative photoionization of $C_2H_5O_2$ measured by Meloni *et al.*,[10] and thus should be ascribed to the contribution of $C_2H_5O_2$.

The neutral $C_2H_5O_2$ at the X^2A'' ground electronic state has an open-shell electronic configuration of $(11a')^2(12a')^2(3a'')^2(13a')^2(4a'')^1$.[34] Theoretical calculations show that removing an electron from the 13a′ orbital or from the 4a″ orbital through photoionization can lead to the X^3A'' ground electronic state or the a^1A' first excited electronic state of $C_2H_5O_2^+$, respectively. The geometric structures of the two conformers of $C_2H_5O_2$, *G*-$C_2H_5O_2$ and *T*-$C_2H_5O_2$, in the X^2A'' ground state are optimized at the M06-2X/aug-cc-pVTZ level of theory and presented in Fig. 3, together with the optimized structures of their individual cations in the X^3A'' and a^1A' electronic states after checking their individual wavefunction stablity.[26] It is shown that *G*-$C_2H_5O_2$ takes a C_1 point-group symmetry and *T*-$C_2H_5O_2$ has a Cs symmetry. For consistency, in the following text we do not change and will still use the symbols X^2A'', X^3A'' and a^1A' (instead of X^2A, X^3A and a^1A) to describe the electronic states of *G*-$C_2H_5O_2$ and its cation. We can see that upon photoionization the structure of the two conformers, *i.e.* their C–O bond length or the CCOO dihedral angle, changes somewhat. This will be discussed in detail in the following paragraphs.

The potential energy curves of the low-lying electronic states of the neutral ethyl peroxy radical (the minimal conformer *G*-$C_2H_5O_2$) and its cation have been calculated at the M06-2X/aug-cc-pVTZ level of theory, and are presented in Fig. 4.[26] Concretely, their structures have been re-optimized at each C–O coordinate and then their energies have been computed. It is shown that the neutral X^2A'' ground state is bound with a C–O equilibrium bond length of 1.446 Å. The cationic X^3A'' ground state of $C_2H_5O_2^+$ is calculated to be a quasi-bound state with a very shallow well and a substantially elongated C–O bond at 2.270 Å, which is out of the Franck–Condon region reached by ionization transitions, as shown using a green rectangle in Fig. 4. The singlet a^1A' first excited state of $C_2H_5O_2^+$ is a bound state with a C–O bond length at 1.687 Å, close to that of the neutral X^2A'' ground state, and should be majorly populated in the photoionization process.

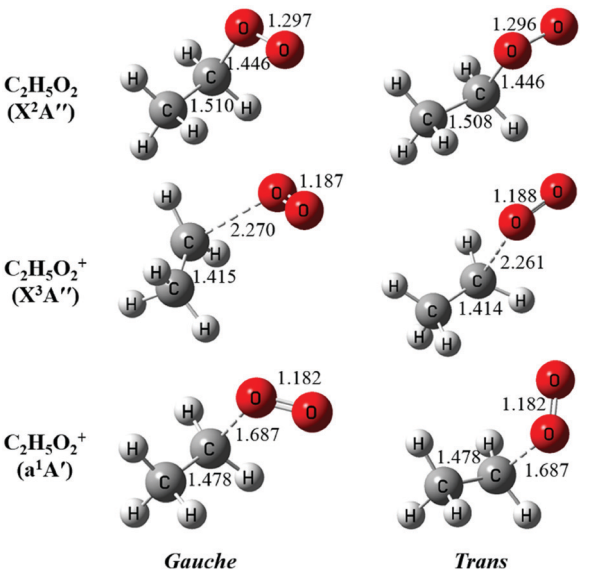

Fig. 3 The optimized structures of the *gauche* and the *trans* conformers of $C_2H_5O_2$ and their cations. The bond lengths are in Å.

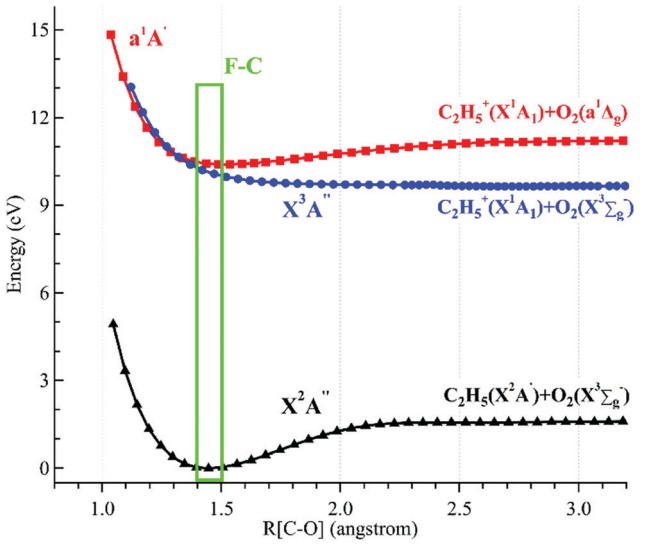

Fig. 4 Potential energy curves of the ethyl peroxy radical (*G*-$C_2H_5O_2$) and its cation along the C–O coordinates. The Franck–Condon (F–C) region is displayed using a green rectangle.

Theoretical calculations in particular using energy and charge distribution analyses show that the cationic X^3A'' ground state adiabatically correlates to the $C_2H_5^+(X^1A_1)$ + $O_2(X^3\Sigma_g^-)$ dissociation limit, and the a^1A' first excited state of $C_2H_5O_2^+$ correlates to the $C_2H_5^+(X^1A_1)$ + $O_2(a^1\Delta_g)$ dissociation limit, not to the $C_2H_5(X^2A')$ + $O_2^+(X^2\Pi_g)$ dissociation limit.[10] In addition, as shown in Fig. 4, the potential energy curve of the a^1A' excited state crosses that of the X^3A'' ground state at ~1.3 Å and their mutual interaction, *e.g. via* the spin–orbit coupling, can cause the singlet a^1A' electronic state to predissociate into $C_2H_5^+$ and O_2 fragments along the potential energy curve of the triplet X^3A'' ground state. This predissociation should be a major reason why the $C_2H_5O_2^+$ cation is not observed and why only the $C_2H_5^+$ fragment ion is observed in the mass spectra.[10,11] In the schematic potential energy diagram of Meloni *et al.*,[10] the a^3A'' repulsive state, which also adiabatically correlates to the $C_2H_5^+(X^1A_1)$ + $O_2(X^3\Sigma_g^-)$ dissociation limit, was proposed to cross with the a^1A' excited state at a larger C–O coordinate and this predissociation might also cause the $C_2H_5O_2^+$ cation to be unstable. Presently the vertical ionization energy (VIE) of the second triplet electronic state, A^3A'', of *G*-$C_2H_5O_2^+$ is calculated to be at 12.24 eV at the TD-M062X/aug-cc-pVTZ level of theory,[26] as listed in Table 1.

The AIEs and the VIEs of the two conformers of $C_2H_5O_2$, corresponding to their individual cationic X^3A'' and a^1A'

Table 1 The ionization energy (IE) of $C_2H_5O_2$ and the appearance energy (AE) of the $C_2H_5^+$ and O_2 fragments in the dissociative photoionization of $C_2H_5O_2$

	State	Species	IE/AE (eV)	Method	Reference
Calc.	X^3A''	$C_2H_5O_2^+$	9.58[a]	QCISD(T)/∞	10
		G-$C_2H_5O_2^+$	9.60[a]/10.40[b]	CCSD(T)-F12/aug-cc-pVTZ	This work
		T-$C_2H_5O_2^+$	9.59[a]/10.39[b]	CCSD(T)-F12/aug-cc-pVTZ	This work
	a^1A'	$C_2H_5O_2^+$	10.01[a]	QCISD(T)/∞	10
		G-$C_2H_5O_2^+$	10.13[a]/10.42[b]	CCSD(T)-F12/aug-cc-pVTZ	This work
		T-$C_2H_5O_2^+$	10.13[a]/10.47[b]	CCSD(T)-F12/aug-cc-pVTZ	This work
	b^1A''	G-$C_2H_5O_2^+$	11.80[b]	TD-M062X/aug-cc-pVTZ	This work
		T-$C_2H_5O_2^+$	11.89[b]	TD-M062X/aug-cc-pVTZ	This work
	A^3A''	G-$C_2H_5O_2^+$	12.24[b]	TD-M062X/aug-cc-pVTZ	This work
		T-$C_2H_5O_2^+$	12.18[b]	TD-M062X/aug-cc-pVTZ	This work
Exp.		$C_2H_5^+$	10.0 $\pm$ 0.1[c]	PIMS	10
		$C_2H_5^+$	10.08 $\pm$ 0.05[c]	PIMS	This work

[a] The adiabatic ionization energy. [b] The vertical ionization energy. [c] The appearance energy.

electronic states, have been calculated at the (R)CCSD(T)-F12/aug-cc-pVTZ level of theory and are listed in Table 1 too, together with the literature data.[10] The calculated AIEs of the two conformers are very close, as the difference between their two cationic states is within 0.01 eV. In addition, the experimental AE of the $C_2H_5^+$ and O_2 fragments is close to the calculated AIE of the a^1A' electronic state of $C_2H_5O_2^+$, in good accordance with the above results of the potential energy curves.

In order to assign the photoionization spectrum in Fig. 2(b), the Franck–Condon factors for the photoionization of $C_2H_5O_2$ have also been calculated at the M062X/aug-cc-pVTZ level.[26] Theoretical calculations show that the G-$C_2H_5O_2$ conformer has favorable Franck–Condon factors in the photoionization transition, from the neutral X^2A'' ground electronic state to the cationic a^1A' first excited state, whereas the Franck–Condon factors of the T-$C_2H_5O_2$ conformer are calculated to be too low to be reliable. The Franck–Condon factors for the transitions to the cationic X^3A'' ground state can be neglected, and its large VIE–AIE difference (0.8 eV), as listed in Table 1, is also an indicator for the negligible ionization cross section. The simulated photoelectron spectrum (PES) of G-$C_2H_5O_2$ is generated from the Franck–Condon factors by convolving the stick spectrum with a Gaussian function (HWHM = 200 cm^{-1}, half width at half-maximum), shown in Fig. S2 (ESI†). The simulated photoionization spectrum is then obtained by the integration of the PES and presented as a blue dotted line in Fig. 2(b). The simulated photoionization spectrum has been energetically shifted ($\sim$90 meV) to match the experimental data. We can see that the simulated photoionization spectrum satisfactorily agrees with the experimental data, although some differences can be observed at higher energy. One possible reason for the discrepancy is that, besides the a^1A' electronic state, the excitations of other higher excited states of G-$C_2H_5O_2^+$ such as the b^1A'' and A^3A'' states listed in Table 1 might also have contributed to the photoionization spectrum at higher energy. Another possible reason is that the experimental photoionization spectrum is directly obtained from the signal of the $C_2H_5^+$ fragment ion and thus its dissociation mechanisms might also have influences on the ion intensity, all of which need to be theoretically investigated in detail in the future.

The above favorable Franck–Condon transition can be understood from the optimized geometric change in the photoionization processes too. Previous theoretical predictions showed that the G-$C_2H_5O_2$ conformer is the minimum with an energy of $\sim$80 cm^{-1} lower than T-$C_2H_5O_2$.[18–21] So under the present experimental conditions ($\sim$298 K), both the G-$C_2H_5O_2$ and T-$C_2H_5O_2$ conformers should have already been prepared and populated in the near effusive gas beam sampling from the fast flow tube at 2 Torr, and then both of them should have contributed to the photoionization spectrum. But, as shown in Fig. 3, for the T-$C_2H_5O_2$ conformer, its C–O bond length of 1.446 Å at the neutral X^2A'' ground state should be increased upon ionization to 2.261 Å at the cationic X^3A'' ground state, or its CCOO dihedral angle of $\pm180^\circ$ at the X^2A'' ground state should be changed to $\pm60^\circ$ at the cationic a^1A' excited state. Our theoretical calculations on the torsional potential energy curves (not presented here) also show that the vertical transition of the T-$C_2H_5O_2$ conformer from the neutral X^2A'' ground state is to the top of the torsional barrier of the cationic a^1A' excited state, whereas the vertical transition of the G-$C_2H_5O_2$ conformer is close to the minima of the a^1A' state. The calculated VIE difference (0.05 eV) of the a^1A' excited state of the two conformers, as listed in Table 1, can somewhat reflect the height of the torsional barrier,[34] which also needs to be studied in detail in the future. These large geometric changes will result in poor Franck–Condon factors and thus will not favor their ionization transitions.

4. Conclusions

In conclusion, we have studied the VUV photoionization of $C_2H_5O_2$ by using a home-made photoionization TOF mass spectrometer at Hefei synchrotron complemented with theoretical calculations. The ethyl peroxy radical was produced in a microwave discharge fast flow tube *via* the reaction of C_2H_5 with oxygen molecules, whereby C_2H_5 was generated *via* the hydrogen-abstraction of ethane with fluorine atoms. The present experiments and theoretical calculations show that the $C_2H_5O_2^+$ cation is not stable and dissociates to $C_2H_5^+$ and O_2

fragments in the photoionization process. Thus, two kinds of $C_2H_5^+$, one from the photoionization of C_2H_5 and one from the dissociative photoionization of $C_2H_5O_2$, have been clearly identified and confirmed in the photoionization mass spectra. The calculated potential energy curves show that the $C_2H_5O_2^+$ cation is firstly prepared at the a^1A' first excited electronic state and then pre-dissociates to the $C_2H_5^+$ and O_2 fragments *via* the spin–orbital coupling of the a^1A' state with the X^3A'' ground state, which is a quasi-bound state with a very shallow well and adiabatically correlates to the $C_2H_5^+$ and O_2 dissociation limit.

The photoionization spectrum corresponding to $C_2H_5O_2$ is obtained and assigned with the aid of the Franck–Condon calculations. Of the two possible conformers for $C_2H_5O_2$, our present findings show that the *G*-$C_2H_5O_2$ conformer has favorable Franck–Condon factors, from the neutral X^2A'' ground state to the cationic a^1A' first excited electronic state, whereas the contribution of the *T*-$C_2H_5O_2$ conformer to the photoionization spectrum is minor or negligible due to its large geometric changes in the photoionization process. The present work provides a prototype using synchrotron-based photoionization mass spectrometry to probe the spectroscopy and structure of peroxy radicals plus their isomers or conformers involved in complex reactions. Some other complex peroxy radicals are being investigated and will be reported in forthcoming papers.

Author contributions

Conception and design: X. T.; acquisition of data: Z. W., X. T., C. W., C. Z., J. Y., and X. G.; theoretical calculation: X. L., B. L., and W. Z.; analysis and interpretation of data: Z. W., X. L., and X. T.; writing—original draft preparation: X. T.; writing—review and editing: all authors; all authors have read and agreed to the published version of the manuscript.

Conflicts of interest

There are no conflicts to declare.

Acknowledgements

This work was financially supported by the National Natural Science Foundation of China (No. 21773249, 91961123, 4212 0104007, U1832184), the International Partnership Program of Chinese Academy of Sciences (No. 116134KYSB20170048) and the Key Program of Research and Development of Hefei Science Center, CAS (No. 2020HSCKPRD001). C. F. is grateful to the Chinese Academy of Sciences President's International Fellowship Initiative (No. 2018VMA0055). The authors are grateful to Dr Jean-Christophe Loison at Univ. Bordeaux, for helpful discussions on the Franck–Condon factors. The authors also would like to thank the NSRL staff for running the synchrotron facility and providing beamtime.

References

1 C. K. Westbrook, Chemical kinetics of hydrocarbon ignition in practical combustion systems, *Proc. Combust. Inst.*, 2000, **28**, 1563–1577.
2 P. S. Monks, Gas-phase radical chemistry in the troposphere, *Chem. Soc. Rev.*, 2005, **34**, 376–395.
3 J. J. Orlando and G. S. Tyndall, Laboratory studies of organic peroxy radical chemistry: an overview with emphasis on recent issues of atmospheric significance, *Chem. Soc. Rev.*, 2012, **41**, 6294–6317.
4 G. Chettur and A. Snelson, Alkylperoxy and alkyl radicals. 4. Matrix IR spectra and UV photolysis of ethylperoxy and ethyl radicals, *J. Phys. Chem.*, 1987, **91**, 3483–3488.
5 G. S. Tyndall, R. A. Cox, C. Granier, R. Lesclaux and G. K. Moortgat, *et al.*, Atmospheric chemistry of small organic peroxy radicals, *J. Geophys. Res.: Atmos.*, 2001, **106**, 12157–12182.
6 E. N. Sharp, P. Rupper and T. A. Miller, The structure and spectra of organic peroxy radicals, *Phys. Chem. Chem. Phys.*, 2008, **10**, 3955–3981.
7 D. B. Atkinson and J. W. Hudgens, Chemical kinetic studies using ultraviolet cavity ring-down spectroscopic detection: self-reaction of ethyl and ethylperoxy radicals and the reaction $O_2 + C_2H_5 \rightarrow C_2H_5O_2$, *J. Phys. Chem. A*, 1997, **101**, 3901–3909.
8 D. B. Atkinson and J. L. Spillman, Alkyl peroxy radical kinetics measured using near-infrared CW-cavity ring-down spectroscopy, *J. Phys. Chem. A*, 2002, **106**, 8891–8902.
9 C. Zhang, M. Shamas, M. Assali, X. Tang and W. Zhang, *et al.*, Absolute absorption cross section of the $\tilde{A} < \text{--}\tilde{X}$ electronic transition of the ethyl peroxy radical and rate constant of its cross reaction with HO2, *Photonics*, 2021, **8**, 296.
10 G. Meloni, P. Zou, S. J. Klippenstein, M. Ahmed and S. R. Leone, *et al.*, Energy-resolved photoionization of alkylperoxy radicals and the stability of their cations, *J. Am. Chem. Soc.*, 2006, **128**, 13559–13567.
11 H. Fu, Y. Hu and E. Bernstein, Generation and detection of alkyl peroxy radicals in a supersonic jet expansion, *J. Chem. Phys.*, 2006, **125**, 014310.
12 K. Voronova, K. M. Ervin, K. G. Torma, P. Hemberger and A. Bodi, *et al.*, Radical thermometers, thermochemistry, and photoelectron spectra: a PEPICO study of the methyl peroxy radical, *J. Phys. Chem. Lett.*, 2018, **9**, 534–539.
13 X. Tang, X. Gu, X. Lin, W. Zhang and G. A. Garcia, *et al.*, Vacuum ultraviolet photodynamics of the methyl peroxy radical studied by double imaging photoelectron photoion coincidences, *J. Chem. Phys.*, 2020, **152**, 104301.
14 F. Qi, Combustion chemistry probed by synchrotron VUV photoionization mass spectrometry, *Proc. Combust. Inst.*, 2013, **34**, 33–63.
15 A. Bodi, P. Hemberger, D. L. Osborn and B. Sztaray, Mass-resolved isomer-selective chemical analysis with imaging photoelectron photoion coincidence spectroscopy, *J. Phys. Chem. Lett.*, 2013, **4**, 2948–2952.

16 X. Tang, X. Lin, G. A. Garcia, J.-C. Loison and C. Fittschen, *et al.*, Threshold photoelectron spectroscopy of the methoxy radical, *J. Chem. Phys.*, 2020, **153**, 031101.
17 X. Tang, X. Lin, G. A. Garcia, J.-C. Loison and Z. Gouid, *et al.*, Identifying isomers of peroxy radicals in the gas phase: 1-$C_3H_7O_2$ vs. 2-$C_3H_7O_2$, *Chem. Commun.*, 2020, **56**, 15525–15528.
18 A. M. Launder, J. M. Turney, J. Agarwal and H. F. Schaefer, Ethylperoxy radical: approaching spectroscopic accuracy *via* coupled-cluster theory, *Phys. Chem. Chem. Phys.*, 2017, **19**, 15715–15723.
19 J. C. Rienstra-Kiracofe, W. D. Allen and H. F. Schaefer, The C_2H_5 + O_2 reaction mechanism: high-level ab initio characterizations, *J. Phys. Chem. A*, 2000, **104**, 9823–9840.
20 G. M. Just, P. Rupper, T. A. Miller and W. L. Meerts, High-resolution cavity ringdown spectroscopy of the jet-cooled ethyl peroxy radical $C_2H_5O_2$, *J. Chem. Phys.*, 2009, **131**, 184303.
21 P. Rupper, E. N. Sharp, G. Tarczay and T. A. Miller, Investigation of ethyl peroxy radical conformers via cavity ring-down spectroscopy of the Ã-X̃ electronic transition, *J. Phys. Chem. A*, 2007, **111**, 832–840.
22 Z. Zhou, X. Du, J. Yang, Y. Wang and C. Li, *et al.*, The vacuum ultraviolet beamline/endstations at NSRL dedicated to combustion research, *J. Synchrotron Radiat.*, 2016, **23**, 1035–1045.
23 Z. Wen, X. Tang, C. Wang, C. Fittschen and T. Wang, *et al.*, A vacuum ultraviolet photoionization time-of-flight mass spectrometer with high sensitivity for study of gas-phase radical reaction in a flow tube, *Int. J. Chem. Kinet.*, 2019, **51**, 178–188.
24 Z. Wen, X. Tang, C. Fittschen, C. Zhang and T. Wang, *et al.*, Online analysis of gas-phase radical reactions using vacuum ultraviolet lamp photoionization and time-of-flight mass spectrometry, *Rev. Sci. Instrum.*, 2020, **91**, 043201.
25 NIST Atomic Spectra Database, https://www.nist.gov/pml/atomic-spectra-database, Accessed June 6, 2021.
26 M. J. Frisch, G. W. Trucks, H. B. Schlegel, G. E. Scuseria and M. A. Robb, *et al.*, *Gaussian 09, Revision A02*, Gaussian, Inc., Wallingford CT, 2016.
27 H.-J. Werner and P. J. Knowles, *MOLPRO version 2015*, http://www.molpro.net.
28 J. D. DeSain, S. J. Klippenstein, J. A. Miller and C. A. Taatjes, Measurements, theory, and modeling of OH formation in ethyl+ O_2 and propyl+ O_2 reactions, *J. Phys. Chem. A*, 2003, **107**, 4415–4427.
29 NIST Chemistry WebBook, http://webbook.nist.gov/chemistry/, Accessed June 6, 2021.
30 B. Ruscic, J. Berkowitz, L. Curtiss and J. Pople, The ethyl radical: Photoionization and theoretical studies, *J. Chem. Phys.*, 1989, **91**, 114–121.
31 B. Gans, G. A. Garcia, S. Boye-Peronne, J.-C. Loison and S. Douin, *et al.*, Absolute photoionization cross section of the ethyl radical in the range 8-11.5 eV: Synchrotron and vacuum ultraviolet laser measurements, *J. Phys. Chem. A*, 2011, **115**, 5387–5396.
32 R. X. Fernandes, K. Luther, G. Marowsky, M. P. Rissanen and R. Timonen, *et al.*, Experimental and modeling study of the temperature and pressure dependence of the reaction C_2H_5+ O_2 (+ M)→ $C_2H_5O_2$ (+ M), *J. Phys. Chem. A*, 2015, **119**, 7263–7269.
33 E. P. Clifford, J. T. Farrell, J. D. DeSain and C. A. Taatjes, Infrared frequency-modulation probing of product formation in alkyl + O2 reactions: I. The reaction of C_2H_5 with O_2 between 295 and 698 K, *J. Phys. Chem. A*, 2000, **104**, 11549–11560.
34 G. E. Quelch, M. M. Gallo and H. F. Schaefer III, Aspects of the reaction mechanism of ethane combustion. Conformations of the ethylperoxy radical, *J. Am. Chem. Soc.*, 1992, **114**, 8239–8247.

